HHS Public Access

Author manuscript

Proc SPIE Int Soc Opt Eng. Author manuscript; available in PMC 2014 May 07.

Published in final edited form as:

Proc SPIE Int Soc Opt Eng. 2013 March 15; 8671: 86711F–. doi:10.1117/12.2008037.

Quantitative Evaluation of Treatment Related Changes on Multi-Parametric MRI after Laser Interstitial Thermal Therapy of Prostate Cancer

Satish Viswanath[a], **Robert Toth**[b], **Mirabela Rusu**[a], **Dan Sperling**[c], **Herbert Lepor**[d], **Jurgen Futterer**[e], and **Anant Madabhushi**[a]

[a]Case Western Reserve University, NJ, USA [b]Rutgers University, NJ, USA [c]New Jersey Institute of Radiology, NJ, USA [d]NYU Langone Medical Center, NY, USA [e]Radboud University Nijmegen Medical Centre, The Netherlands

Abstract

Laser interstitial thermal therapy (LITT) has recently shown great promise as a treatment strategy for localized, focal, low-grade, organ-confined prostate cancer (CaP). Additionally, LITT is compatible with multi-parametric magnetic resonance imaging (MP-MRI) which in turn enables (1) high resolution, accurate localization of ablation zones on *in vivo* MP-MRI prior to LITT, and (2) real-time monitoring of temperature changes *in vivo* via MR thermometry during LITT. In spite of rapidly increasing interest in the use of LITT for treating low grade, focal CaP, very little is known about treatment-related changes following LITT. There is thus a clear need for studying post-LITT changes via MP-MRI and consequently to attempt to (1) quantitatively identify MP-MRI markers predictive of favorable treatment response and longer term patient outcome, and (2) identify which MP-MRI markers are most sensitive to post-LITT changes in the prostate. In this work, we present the first attempt at examining focal treatment-related changes on a per-voxel basis (high resolution) via quantitative evaluation of MR parameters pre- and post-LITT. A retrospective cohort of MP-MRI data comprising both pre- and post-LITT T2-weighted (T2w) and diffusion-weighted (DWI) acquisitions was considered, where DWI MRI yielded an Apparent Diffusion Co-efficient (ADC) map. A spatially constrained affine registration scheme was implemented to first bring T2w and ADC images into alignment within each of the pre- and post-LITT acquisitions, following which the pre- and post-LITT acquisitions were aligned. Pre- and post-LITT MR parameters (T2w intensity, ADC value) were then standardized to a uniform scale (to correct for intensity drift) and then quantified via the raw intensity values as well as via texture features derived from T2w MRI. In order to quantify imaging changes as a result of LITT, absolute differences were calculated between the normalized pre- and post-LITT MRI parameters. Quantitatively combining the ADC and T2w MRI parameters enabled construction of an integrated MP-MRI difference map that was highly indicative of changes specific to the LITT ablation zone. Preliminary quantitative comparison of the changes in different MR parameters indicated that T2w texture may be highly sensitive as well as specific in identifying changes

Correspondence to sev21@case.edu, axm788@case.edu.

within the ablation zone pre- and post-LITT. Visual evaluation of the differences in T2w texture features pre- and post-LITT also appeared to provide an indication of LITT-related effects such as edema. Our preliminary results thus indicate great potential for non-invasive MP-MRI imaging markers for determining focal treatment related changes, and hence long- and short-term patient outcome.

Keywords

laser interstitial thermal therapy; prostate cancer; focal treatment; treatment change; registration; multi-parametric MRI

1. INTRODUCTION

Prostate cancer (CaP) is the most frequent malignancy diagnosed in men 50 years and older in industrialized countries.[1] Recent improvements in localization and detection protocols has led to an increase in the number of prostate cancers found; a growing fraction of which are small foci (of potentially low-grade) CaP being diagnosed in healthy young men. However, the lifetime risk of mortality due to CaP is estimated to be less than 10%,[2] hence, while 1 in 6 men may be diagnosed with prostate cancer, only 1 in 36 will die from it.[1] While active surveillance is finding increasing popularity in patients with more focal, lower grade CaP by allowing monitoring for signs of metastasis, most patients prefer to undergo some form of radical treatment (prostatectomy, radiation treatment) despite significant morbidity (urinary, sexual dysfunction).[1]

Recent studies have observed that CaP occurs both unifocally and multi-focally within the prostate. This has led to the definition of the *index lesion* as the largest focus of CaP as measured by volume, within the prostate.[3] Most secondary (non-index) tumors have exhibited relatively small volumes and have rarely had a higher Gleason score than the index lesion; both of which make them unlikely to affect overall disease progression.[4] Thus, biologically speaking, most patients can be considered to have unifocal disease (i.e. the index lesion), by targeting which one can dramatically decrease total tumor volume and eliminate the most likely source of metastasis.[5] A viable solution to this lies in focal therapy strategies which additionally reduce overtreatment of CaP in the general population, while allowing patients to have their disease treated once diagnosed.[1]

Different focal therapy strategies are being explored for current clinical use including laser interstitial thermal therapy (LITT), high intensity focused ultrasound (HIFU), cryotherapy, and photo-dynamic therapy (PDT). Both HIFU and LITT involve thermal destruction of tissue by either using tightly focused ultrasound energy delivered via a transrectal probe (HIFU) or via the Nd-YAG laser delivered by an interstitial fiber (LITT). Depending on the amount of heat energy delivered and depth of penetration, the temperature is raised in the tissue where rapid coagulative necrosis and instant cell death occur above 60° C. Cryotherapy utilizes a transperineal probe to lower the temperature within the tissue causing cell membrane disruption, necrosis, and vascular thrombosis. PDT utilizes an administered photosensitizer that accumulates in target tissue and is activated by light to generate active radicals that are toxic to the tissue. Of these, LITT has emerged as the most promising

solution for a number of different diseases[6] due to (1) lack of precision for cryotherapy for focal ablation with minimal disruption of normal function,[4] (2) experimental nature of PDT leading to significant side-effects and adjuvent hormonal therapy,[7] and (3) typical whole-gland ablation procedure of HIFU due to difficulty targeting specific areas within the prostate using ultrasound.[8]

One of the major advantages enjoyed by LITT is its compatibility with magnetic resonance imaging (MRI), allowing for high resolution *in vivo* imaging to be used in LITT procedures.[9] LITT is uniquely suited for use and direct integration with MRI due to (1) use of quartz fibers which do not cause any disturbance during imaging, and (2) non-electromagnetic energy being used for LITT. In comparison, alternative focal therapy solutions (cryotherapy, HIFU) require modifications to underlying technology to prevent electromagnetic disturbance or require the MR scanning to be stopped in order to perform treatment. MRI is also capable of monitoring temperature change in the tissue, which enables real-time monitoring of LITT. Further, multi-parametric MRI (MP-MRI) offers the ability to accurately denote the specific location of biopsy-proven CaP within the gland,[1] which is very important for accurately delineating ablation zones within the prostate as well as for accurate guidance of the laser fiber during treatment. The prostate is well-suited for this form of treatment due to an optimal heat conduction rate (optical absorption) as well as low vasculature (which can limit the ablation size).[1]

Recent clinical studies examining the technical feasibility of LITT for focal treatment of CaP have reported negligible post-operative morbidity.[1] However, there is very little work describing the specific *in vivo* imaging characteristics of LITT-induced changes in the prostate. This implies a need for better co-registration and image analysis methods for quantitatively comparing pre- and post-LITT MP-MRI, in order to identify voxel-by-voxel changes in MP-MRI markers that can in turn describe LITT-related changes within the prostate. Further, MP-MRI markers need to be quantitatively evaluated for their sensitivity to changes in the prostate following LITT. Examining quantitative changes to these imaging markers as a function of time may also later be correlated with long-term disease and patient prognosis.

2. PREVIOUS RELATED WORK AND OBJECTIVES OF THE CURRENT WORK

The effects of radiation treatment (RT) in the prostate have been qualitatively examined in a number of studies.[10–14] Comparison of the pre- and post-RT MP-MR imaging acquisitions have shown that successful RT of CaP on MRI is characterized by uniform T2-weighted (T2w) signal intensity without focal abnormalities, while locally recurrent CaP is characterized by hypo-intense regions of smooth texture.[11] Similarly, post-RT diffusion-weighted imaging (DWI) shows an overall increase in ADC values within the entire prostate when CaP is successfully treated. Unchanged or decreased ADC values correspond to locally recurrent CaP.[10] Our group[15, 16] has leveraged these qualitative characteristics within novel quantitative schemes for per-voxel evaluation and MP-MRI signature construction to differentiate between possible RT outcomes (success, unsuccessful, recurrence). This was done by calculating absolute differences between different MP-MRI

parameters; these differences were found to be highly indicative of RT-related changes and treatment effects within the prostate. More significantly, as different MP-MRI parameters quantify different types of treatment-related information, the combination of MP-MRI imaging markers was found to outperform any individual marker for detecting RT-related changes within the prostate.

In organs such as the liver, the extent of tissue necrosis due to LITT has been shown to be visible on MRI.[17] In a recent Phase I LITT trial involving CaP patients, good correlation was found between volumes of thermal damage that were visible on MRI and those determined via staining of *ex vivo* surgical prostatectomy specimens from patients who had previously undergone LITT.[18] Rosenkrantz et al[9] have described some of the primary imaging characteristics at the 6-month follow-up mark after most types of focal therapy (though this study was not limited to LITT). The most significant of these was a decrease in the prostate volume (leading to loss of differentiation between prostatic zones), as well as poor visualization of the capsule. To our knowledge, the relative importance and utility of different MP-MRI protocols in determining post-LITT effects has not been explored in detail. For example, structural T2w MRI is considered to be of limited utility to evaluate focal therapy effects due to presence of multifocal hypointensities that appear due to prostatic parenchyma.[9] By contrast, dynamic contrast enhanced MRI (DCE MRI) may be highly sensitive (but not necessarily specific) for detecting CaP recurrence around any focal ablation zone. However, areas of benign hypertrophy may show hypervascularity which can limit the specificity of DCE MRI (hypertrophy seen as false positive enhancement).[9] Diffusion weighted imaging (DWI) may augment specificity of detecting recurrent tumors, but has not been explored in great detail. These largely qualitative observations of LITT-related changes on prostate MP-MRI are likely highly prone to observer error, hence, the use of quantitative image analysis tools may help interpret prostate MP-MRI in a consistent, reproducible fashion,[19] and possibly improve our understanding of LITT-related changes on MP-MRI.

In this work, we present the first attempt at quantitative image analysis of high-resolution (per-voxel) evaluation of treatment-related changes *in vivo* in patients who have undergone LITT, using MP-MRI. We believe that a quantitative approach to evaluation of treatment-related changes between pre- and post-LITT MP-MRI may also allow for the building of a novel imaging-based prognostic indicators of patient treatment response. We utilize a retrospective cohort of MP-MRI data that comprises both pre- and post-LITT acquisitions, including T2-weighted (T2w) and diffusion-weighted (DWI) protocols was considered, where an Apparent Diffusion Coefficient (ADC) map is calculated from DWI MRI. A spatially constrained affine registration scheme[16, 20] will be used to first bring the T2w and ADC images into alignment within each of the pre- and post-LITT acquisitions, following which the pre- and post-LITT acquisitions will be aligned. Pre- and post-LITT MR parameters (T2w intensity, ADC value) will then be standardized to correct for intensity drift between acquisitions,[20] following which they will be quantified in terms of the raw intensity values as well as via texture features derived from T2w MRI.[19, 21] In order to quantify imaging changes as a result of LITT, absolute differences will be calculated between the normalized pre- and post-LITT MRI parameters. This will enable quantitative

comparision of sensitivity and specificity of different MP-MRI parameters in detecting changes within the ablation zone as a result of LITT, as well as examine the performance of integrating MP-MRI parameters to construct a combined quantitative signature of LITT-related effects within the prostate. A deeper understanding of imaging-related changes due to LITT can also enable comparisons between radical (e.g. radiation treatment) and focal (e.g. LITT) therapy options for CaP. The remainder of this paper is organized as follows. Section 3 illustrates the experimental design, while Section 4 summarizes the experimental results and associated discussion. Finally, Section 5 presents our concluding remarks.

3. EXPERIMENTAL DESIGN

3.1 Data Description

A cohort of 5 patient studies were obtained from the New Jersey Institute of Radiology. Prior to initial MR imaging, all patients had been confirmed to have organ localized prostate cancer with Gleason scores between 6 and 7 (based on core-needle biopsies, no single core had > 50% involvement). Final treatment outcome for all 5 patients was determined as successful with no local recurrence or residual CaP seen on follow-up (during the post-LITT MP-MRI exam), as well as low PSA. Annotations of the ablation zone (CaP) as well as benign regions (normal) on the pre-LITT T2w MRI were obtained via an expert radiologist who delineated the ablation zone (AZ) by considering the MR image appearance of the AZ and the location of the needle during treatment. Care was taken to ensure that the CaP and normal regions were separated out as best possible based off visual observation of the AZ.

3.2 Pre- and post-LITT MP-MRI acquisition

For each patient, pre- and post-LITT MP-MRI scans included T2w and DWI protocols. All studies were performed using a Siemens Symphony 1.5 Tesla MRI machine together with a whole-body coil for excitation, as well as the current Medrad inflatable endorectal coil in conjunction with a pelvic phase array coil for signal reception.

T2w imaging comprised thin-section high-resolution oblique, axial, and coronal fast spin-echo images of the prostate and seminal vesicles. Imaging parameters were TR/TE = 4000–6000/90–120 msec, echo train length = 8–16, slice thickness = 3 mm, interslice gap 0 mm, matrix size of 256 × 192, with 3 excitation and field of view of 14 cm. ADC maps were calculated from a set of oblique axial DTI-EPI images with 6 diffusion gradient directions with a FOV of 24 cm, 256 × 128 matrix, 4mm thick slices (8–10 slices typically cover the prostate), and *b*-values of 0 and 600.

Each patient underwent an MRI-guided LITT procedure using Visualase Thermal Therapy System (Visualase Inc, Houston, TX) between 1 and 4 months after the initialMP-MRI acquisition. This system comprises a surgical diode laser, a fiber-optic laser applicator with diffusing tip and a coaxial cooling catheter, a cooling circulation pump, and a computer workstation for processing and display of MR images. During LITT, laser applicator placement was performed using the Invivo DynaTRIM transrectal biopsy guidance system (Invivo, Pewaukee, WI). The post-LITT MP-MRI (T2w, DWI) scan was acquired for each patient between 3 and 4 months after the LITT procedure.

3.3 Notation

We define $\mathscr{C}_{\beta}^{pre}=(C, f_{\beta}^{pre})$ as the pre-LITT MR scene, where β = {*t2w*, *adc*} corresponds to the different MR protocols, and $f_{\beta}^{pre}(c)$ is the T2w or ADC value associated with every voxel *c* in a 3D grid *C*. The region annotated as the ablation zone (CaP) is denoted *A*(*C*) while the normal, benign annotation is denoted *N*(*C*).

3.4 Alignment of pre-, post-LITT T2w MRI

Registration of the pre-LITT T2w prostate image scene $(\mathscr{C}_{t2w}^{pre})$ to the post-LITT T2w prostate MRI scene $(\hat{\mathscr{C}}_{t2w}^{post})$ is required in order to compare MR parameters before and after LITT, on a per-voxel basis. Post- to pre-LITT registration is performed using the T2w protocol as it helps to visualize internal prostatic structures with excellent resolution, enabling accurate image registration.

Post- to pre-LITT registration is accomplished using a spatially constrained normalized mutual information (NMI) similarity measure.[22] The original MR volume is cropped to contain the prostate alone, and NMI is calculated within this area in order to drive the registration. NMI was chosen to drive the registration procedure due to its robustness to non-linear intensity relationships.[22] This measure is used to drive a 3D affine transformation of $\hat{\mathscr{C}}_{t2w}^{post}$ onto $\mathscr{C}_{t2w}^{pre}$ with 12 degrees of freedom, encoding for image rotation, translation, shearing, and scale. This transformation is able to account for the major changes to the prostate region as a result of LITT,[9] including acquisition-based differences, patient movement, and changes to the prostate appearance. As a result of registration, the aligned post-LITT T2w MRI scene is obtained as,

$$\mathscr{C}_{t2w}^{post}=\mathbf{T}^{pp}\times\hat{\mathscr{C}}_{t2w}^{post}, \quad (1)$$

via the 3D affine transformation $\mathbf{T}^{pp}$ (transforming post-LITT T2w MRI to pre-LITT T2w MRI). Figure 1(a) allows for visualization of image registration of $\hat{\mathscr{C}}_{t2w}^{post}$ to $\mathscr{C}_{t2w}^{pre}$ in the form of a checkerboard pattern, where alternating squares correspond to images from each of $\mathscr{C}_{t2w}^{pre}$ and $\mathscr{C}_{t2w}^{post}$. The contiguity of structures corresponding to prostatic zones, zonal boundaries, and nodules within the prostate capsule (red outline) suggest a successful registration accounting for the major changes to the prostate as a result of LITT.

3.5 Inter-protocol alignment of T2w, DWI MRI

Within each MR acquisition, the ADC map must be brought into spatial alignment with the corresponding T2w MR scene (e.g. $\tilde{\mathscr{C}}_{adc}^{pre}$ to $\mathscr{C}_{t2w}^{pre}$), to correct for voxel size and resolution differences as well as artifacts due to calculation of the ADC map from the original DWI MRI. This registration enables the building of a combined multi-parametric MR signature which integrates both T2w and DWI information to uniquely quantify changes to the prostate as a result of LITT. This is done via volumetric affine registration driven by a spatially constrained NMI measure, as described in Section 3.4, to yield

$$\mathscr{C}_{adc}^{pre} = \mathbf{T}^{pre} \times \tilde{\mathscr{C}}_{adc}^{pre}, \quad (2)$$

via the 3D affine transformation $\mathbf{T}^{pre}$ (transforming pre-LITT ADC to pre-LITT T2w MRI).

The post-LITT ADC map involves a two-step registration process where it is first brought into alignment with $\hat{\mathscr{C}}_{t2w}^{post}$, followed by a second transformation to bring it into alignment with $\mathscr{C}_{t2w}^{pre}$, i.e.

$$\mathscr{C}_{adc}^{post} = \mathbf{T}^{pp}\mathbf{T}^{post} \times \tilde{\mathscr{C}}_{adc}^{post}, \quad (3)$$

where $\mathbf{T}^{post}$ transforms post-LITT ADC to post-LITT T2w MRI, followed by $\mathbf{T}^{pp}$ to align it to the pre-LITT T2w MRI. All MRI data is thus transformed into the pre-LITT T2w MRI co-ordinate frame *C* and field of view (FOV, 512 × 512 voxels).

Figure 1(b) allows for visualization of the registration result of $\tilde{\mathscr{C}}_{adc}^{pre}$ to $\mathscr{C}_{t2w}^{pre}$ in the form of a checkerboard, where alternating squares correspond to images from each of $\mathscr{C}_{adc}^{pre}$ and $\mathscr{C}_{t2w}^{pre}$. The contiguity of structures corresponding to prostatic zones, zonal boundaries, and nodules within the prostate capsule (red outline) suggest a successful registration accounting for voxel size and resolution differences between the 2 protocols.

3.6 Pre-processing of pre- and post-LITT MP-MRI

The MR acquisitions pre- and post-LITT were not found to suffer from MR bias field intensity inhomogeneity[23] but did suffer from intensity drift and non-standardness.[20] MR intensity non-standardness implies that grayscale intensities do not have a fixed tissue-specific meaning within the same imaging protocol, the same body region, or even within the same patient.[20] When the histograms for $\mathscr{C}_{t2}^{pre}$ (red) and $\mathscr{C}_{t2}^{post}$ (blue) are plotted together (Figure 1(c)), it is clear they have different intensity ranges and are not in alignment. In order to quantitatively compare the changes in MR parameters between pre- and post-LITT acquitions, the Nyul and Udupa algorithm[24] was implemented to automatically identify corresponding landmarks on each of the histograms, and non-linearly map them to one other. As a result of intensity standardization, the histograms are aligned (Figure 1(d)) and the MR parameters can be directly compared. Intensity standardization was performed for corresponding pairs of protocols $(\mathscr{C}_{t2}^{post}/\mathscr{C}_{t2}^{pre}, \mathscr{C}_{adc}^{pre}/\mathscr{C}_{adc}^{post})$ between pre- and post-LITT MRI acquisitions.

The prostate capsule was segmented out of the larger $\mathscr{C}_{t2w}^{pre}$ FOV by an expert radiologist. This segmentation is applied to each of $\mathscr{C}_{t2w}^{pre}$, $\mathscr{C}_{t2w}^{post}$, $\mathscr{C}_{adc}^{pre}$, and $\mathscr{C}_{adc}^{post}$ in order to restrict all analysis to within the prostate region-of-interest alone.

3.7 Quantification of MP-MRI via texture features

In addition to utilizing the raw T2w $(f_{t2w}^{pre}, f_{t2w}^{post})$ and ADC $(f_{adc}^{pre}, f_{adc}^{post})$ intensity value as a parametric representation of MP-MRI information, texture features have been widely shown

to be highly effective in characterizing the prostate appearance in order to differentiate between regions within the prostate.[19, 25]

A total of 28 texture features previously shown to improve differentiation between CaP and benign regions[19, 21] were extracted from each of $\mathscr{C}_{t2w}^{pre}$ and $\mathscr{C}_{t2w}^{post}$, on a per-voxel basis. These features are obtained by (1) calculating responses to various filter operators, and (2) computing gray level intensity co-occurrence statistics, as follows,

- *Non-steerable gradient features*: Eight non-steerable gradient features were obtained by convolving Sobel and Kirsch edge filters and first-order spatial derivative operators with $\mathscr{C}_{t2w}^{pre}$ and $\mathscr{C}_{t2w}^{post}$. These operators allow for detection of the strength of horizontal, vertical, and diagonal edges within the image using linear kernels.[26]
- *Steerable gradient features*: Gabor operators comprise the steerable class of gradient calculations which attempt to match localized frequency characteristics.[27] A Gabor filter can be defined as the modulation of a complex sinusoid by a Gaussian function and is controlled by scale, bandwidth, and frequency parameters. A total of 8 Gabor features were calculated based on responses to convolving $\mathscr{C}_{t2w}^{pre}$ and $\mathscr{C}_{t2w}^{post}$ with distinct Gabor operators obtained by varying each of the associated parameters.
- *Second order statistical features*: Second order statistical features have been proposed by Haralick[28] and have found wide application in computing features with perceptual meaning for computerized detection systems.[19, 21] These features are based on quantifying the spatial gray-level co-occurrence within local neighborhoods around each pixel in an image, stored in the form of matrices. 13 Haralick features were calculated based on statistics derived from these matrices for $\mathscr{C}_{t2w}^{pre}$ and $\mathscr{C}_{t2w}^{post}$.

The reader is directed to [19,21] for a more detailed description of the individual texture features. Feature extraction results in feature scenes $\mathscr{F}_{\varphi}^{\kappa}=(C, f_{\varphi}^{\kappa})$, where $f_{\varphi}^{\kappa}(c)$ is the feature value at location $c \in C$ when feature operator ϕ is applied to scene $\mathscr{C}_{t2w}^{\kappa}, \kappa \in \{pre, post\}$. For ease of notation, the raw T2w intensity value and ADC value are included in this set of feature scenes, i.e. ϕ can correspond to $\{t2w, adc\}$ in addition to the T2w texture features that are then subsequently extracted.

3.8 Quantifying LITT-related changes in individual MP-MRI parameters

For each MR parameter considered, the range of values are normalized to have a mean of 0 and a mean absolute deviation of 1. This ensures that the different parameter values lie in a comparable range of values when quantifying differences in pre- and post-LITT MP-MRI.

Two statistics within the annotated regions $A(C)$ and $N(C)$ specifically were calculated This is done to ensure that false positives such as edema are not taken into account when observing changes within the CaP region due to LITT.

The actual change in the MP-MRI parameter values as a result of LITT is calculated as the mean MP-MRI normalized parameter value within each of $A(C)$ and $N(C)$ for $\kappa \in \{pre, post\}$ respectively, and for each feature ϕ,

$$\Delta_{\varphi}^{A,\kappa}=\frac{1}{|A(C)|}\sum_{c\in A(C)}, f_{\varphi}^{\kappa}(c) \quad (4)$$

$$\Delta_{\varphi}^{N,\kappa}=\frac{1}{|N(C)|}\sum_{c\in A(C)}\cdot f_{\varphi}^{\kappa}(c) \quad (5)$$

The absolute percentage change within each of $A(C)$ and $N(C)$ with respect to the pre-LITT MP-MRI parameter values allows for determination of how sensitive or specific each MP-MRI parameter truly is to demonstrating large changes within $A(C)$ and small changes within $N(C)$. This is quantified as,

$$\rho_{\varphi}^{A}=\frac{1}{|A(C)|}\sum_{c\in A(C)}\frac{\delta_{\varphi}(c)}{f_{\varphi}^{pre}(c)} \quad (6)$$

$$\rho_{\varphi}^{N}=\frac{1}{|N(C)|}\sum_{c\in N(C)}\frac{\delta_{\varphi}(c)}{f_{\varphi}^{pre}(c)} \quad (7)$$

3.9 Weighted difference map of MP-MRI markers

The L_1 norm difference between the normalized pre- and post-LITT MP-MRI feature values is then calculated as

$$\delta_{\varphi}(c)=f_{\varphi}^{pre}(c)-f_{\varphi}^{post}(c), \quad (8)$$

for every voxel $c \in C$. $\mathscr{D}_{t2w}$ is thus the 3D T2w intensity difference scene while $\mathscr{D}_{adc}$ is the ADC value difference scene. Similarly difference scenes can be defined for all the other feature scenes described in Section 3.7. A weighted MP-MRI difference map based on the raw parameter values is constructed as,

$$\mathscr{D}_{int}=\alpha_{t2w}|\mathscr{D}_{t2w}|+\alpha_{adc}|\mathscr{D}_{adc}|, \quad (9)$$

where $\alpha_{t2w} + \alpha_{adc} = 1$, $0 \le \alpha_{t2w} \le 1$, $0 \le \alpha_{adc} \le 1$. α_{t2w}, α_{adc} were obtained via a grid search strategy where each weight was varied between 0 and 1 in steps of 0.1, and the corresponding difference map was evaluated for sensitivity and specificity with respect to the annotated $A(C)$ and $N(C)$. The scene demonstrating the best correspondence was retained to construct $\mathscr{D}_{int}$.

Difference scenes can be visualized within the prostate ROI while utilizing a colormap, such that blue corresponds to small difference values and red corresponds to areas of high differences. It may be expected that regions within $A(C)$ will show large differences between

pre- and post-LITT MP-MRI parameters i.e. significant change due to treatment, while regions denoted by $N(C)$ show little to no change due to treatment. Note that this observation cannot be generalized to the entire prostate, as effects such as edema among other reactions to treatment may also cause changes to the MP-MRI parameters.[1, 9]

4. EXPERIMENTAL RESULTS AND DISCUSSION

4.1 Comparing the integrated MP-MRI difference map to individual MRI protocol difference maps

Figure 2 illustrates representative results from 2 different datasets for $\mathscr{D}_{t2w}$, $\mathscr{D}_{adc}$, and $\mathscr{D}_{int}$. Comparing against the ablation zone for each study, based on the location of the Visualase needle in Figures 2(a) and (e), the integrated 3D weighted MP-MRI difference scenes (Figures 2(d) and (h)) are seen to demonstrate distinct change (reddish orange) that is highly specific to the successfully treated CaP region. By comparison the individual protocol difference maps are not consistently as specific in visualizing distinct change, as seen in the false positive regions in Figures 2(c) and (f).

4.2 Visualizing imaging changes due to LITT on MP-MRI

Figure 3 illustrates the qualitative change in different MP-MRI parameters within $A(C)$ (red) and $N(C)$ (green). It is clear that the original T2w MRI (Figures 3(a) and (d)) do not show a distinct change within the CaP region, but the benign region has a consistent appearance. This is likely because diffuse T2w appearance is commonly observed after most types of treatment,[9, 11] causing confounders between the appearance of CaP and successfully treated CaP regions. The original ADC maps (Figures 3(b) and (e)) show a distinct brightening within the CaP region, but an inconsistent response within the benign region. The visualized ADC change within the CaP region may be explained by the fact that loss of cell membrane integrity (early process of cell death) and necrosis cause an increase in water mobility,[29] which would result in an increase in the ADC value in that region.

The T2w texture feature (Haralick energy), selected as it demonstrated the largest change within $A(C)$ and the smallest change within $N(C)$, can be seen to: (1) demonstrate a similar response pre- and post-LITT within $N(C)$ (green outline, low change), (2) different responses pre- and post-LITT within $A(C)$ (red outline, high change), as well as (3) visualize reaction by the tissue to the LITT procedure as a distinct (over-expression) response that is localized around the AZ. Haralick energy attempts to quantify how heterogeneous the tissue appearance is and hence how smooth the variation in intensity values are. We have previously shown that such features demonstrate a response specific to peripheral zone tumors,[19] which would explain why this feature demonstrates a distinct change after successful LITT ablation (due to absence of tumor post-LITT). Additionally, there appears to be a non-smooth variation in T2w intensities that is visually indiscernible in Figures 3(a), (d) but has been expressed by this feature, which we believe may imply the presence of edema or a similar LITT-related change which may be expected to occur as a result of ablation.[9]

4.3 Comparison of MP-MRI markers in quantifying LITT-related changes

Table 4(a) summarizes the quantitative measures of LITT-related change within different MP-MRI parameters. Note that the values in this table are normalized values within each of $A(C)$ and $N(C)$ for 3 different MR parameters, averaged over all 5 datasets. The percent absolute difference between each parameter in Table 4(a) is visualized as a bar graph in Figure 4(b) (averaged over all 5 datasets). These quantitative measures appear to reflect the qualitative observations in Figure 3. While the ADC value shows the largest percent change between pre- and post-LITT acquisitions, this change is seen in both cancerous and normal regions, implying that it is sensitive but not specific. By comparison, the T2w intensity value shows the lowest percent change between pre- and post-LITT MP-MRI acquisitions, demonstrating a marginally improved specificity over the ADC value. However, T2w texture appears to provide an excellent trade-off between sensitivity and specificity, exhibiting a distinct change within cancerous regions and a lower change within benign regions.

5. CONCLUDING REMARKS

Laser interstitial thermal therapy (LITT) is a highly promising focal strategy for low-grade, organ-confined prostate cancer, further enhanced by its ease of integration with high resolution MP-MR imaging. In order for LITT to gain popularity as a treatment strategy, it is important to be able to qualify and quantify LITT treatment success in comparison to more popular, albeit morbid, radical treatment options (e.g. radiation therapy). In this work, we have presented preliminary results of evaluating treatment-related changes *in vivo* after LITT in the case of prostate cancer patients. Our initial results based on 5 patient studies indicate that the integration of T2w and ADC may yield a difference signature that both accurately models treatment-related changes post-LITT, as well as outperforms the individual T2w and ADC parameters in this regard. ADC maps demonstrated highly sensitive, albeit non-specific, response to LITT-related changes *in vivo*, due to the significant change in water permeability in tissue as a result of treatment. By comparison, T2w MRI was inconsistent in demonstrating LITT-related change, possibly due to diffuse T2w appearance post-therapy. Additionally, T2w texture was found to be both sensitive and specific to visualizing and quantifying (a) effects of successfully ablating the CaP regions as well as (b) providing an indication of additional treatment related changes such as edema. This may be because these features quantify visually indiscernible heterogeneous appearance of tissue as well as demonstrating both highly sensitive and specific responses to each of benign and cancerous regions. Future work will involve validation of our findings on a larger cohort of data as well as validation of the MP-MRI imaging markers in being prognostic of long-term patient outcome.

ACKNOWLEDGMENTS

This work was made possible by grants from the National Institute of Health (R01CA136535, R01CA140772, R43EB015199, R21CA167811), National Science Foundation (IIP-1248316), and the QED award from the University City Science Center and Rutgers University.

REFERENCES

1. Colin P, Mordon S, Nevoux P, Marqa M, Ouzzane A, Puech P, Bozzini G, Leroux B, Villers A, Betrouni N. Focal laser ablation of prostate cancer: definition, needs, and future. Adv Urol. 2012; 2012:589160. [PubMed: 22666240]
2. Lindner U, Weersink RA, Haider MA, Gertner MR, Davidson SR, Atri M, Wilson BC, Fenster A, Trachtenberg J. Image guided photothermal focal therapy for localized prostate cancer: phase I trial. J Urol. 2009; 182(4):1371–1377. [PubMed: 19683262]
3. Wise AM, Stamey TA, McNeal JE, Clayton JL. Morphologic and clinical significance of multifocal prostate cancers in radical prostatectomy specimens. Urology. 2002; 60(2):264–269. [PubMed: 12137824]
4. Eggener SE, Scardino PT, Carroll PR, Zelefsky MJ, Sartor O, Hricak H, Wheeler TM, Fine SW, Trachtenberg J, Rubin MA, Ohori M, Kuroiwa K, Rossignol M, Abenhaim L. Focal Therapy for Localized Prostate Cancer: A Critical Appraisal of Rationale and Modalities. The Journal of Urology. 2007; 178(6):2260–2267. [PubMed: 17936815]
5. Ahmed HU. The Index Lesion and the Origin of Prostate Cancer. New England Journal of Medicine. 2009; 361(17):1704–1706. [PubMed: 19846858]
6. Stafford J, Fuentes D, Elliott AA, Weinberg JS, Ahrar K. Laser-induced thermal therapy for tumor ablation. Critical Reviews in Biomedical Engineering. 2010; 38(1):79. [PubMed: 21175405]
7. Nathan TR, Whitelaw DE, Chang SC, Lees WR, Ripley PM, Payne H, Jones L, Parkinson MC, Emberton M, Gillams AR, Mundy AR, Bown SG. Photodynamic Therapy for Prostate Cancer Recurrence After Radiotherapy: A Phase I Study. The Journal of Urology. 2002; 168(4, Part 1): 1427–1432. [PubMed: 12352410]
8. Uchida T, Ohkusa H, Nagata Y, Hyodo T, Satoh T, Irie A. Treatment of localized prostate cancer using high-intensity focused ultrasound. BJU International. 2006; 97(1):56–61. [PubMed: 16336329]
9. Rosenkrantz A, Scionti S, Mendrinos S, Taneja S. Role of MRI in minimally invasive focal ablative therapy for prostate cancer. AJR Am J Roentgenol. 2011; 197(1):W90–W96. [PubMed: 21701001]
10. Song I, Kim C, Park B, Park W. Assessment of Response to Radiotherapy for Prostate Cancer: Value of Diffusion-Weighted MRI at 3 T. Am. J. Roentgenol. 2010; 194(6):W477–W482. [PubMed: 20489065]
11. Westphalen A, Kurhanewicz J, Cunha R, Hsu I, Kornak J, Zhao S, Coakley F. T2-Weighted endorectal magnetic resonance imaging of prostate cancer after external beam radiation therapy. Int Braz J Urol. 2009; 35(2):171–180. [PubMed: 19409121]
12. Pucar D, Sella T, Schoder H. The role of imaging in the detection of prostate cancer local recurrence after radiation therapy and surgery. Curr Opin Urol. 2008; 18(1):87–97. [PubMed: 18090496]
13. Pickett B, Kurhanewicz J, Coakley F, Shinohara K, Fein B, Roach M. Use of MRI and spectroscopy in evaluation of external beam radiotherapy for prostate cancer. Int J Radiat Oncol Biol Phys. 2004; 60(4):1047–1055. [PubMed: 15519774]
14. Coakley F, Teh H, Qayyum A, Swanson M, Lu Y, Roach M, Pickett B, Shinohara K, Vigneron D, Kurhanewicz J. Endorectal MR imaging and MR spectroscopic imaging for locally recurrent prostate cancer after external beam radiation therapy: preliminary experience. Radiology. 2004; 233(2):441–448. [PubMed: 15375223]
15. Tiwari P, Viswanath S, Kurhanewicz J, Madabhushi A. Weighted Combination of Multi-Parametric MR Imaging Markers for Evaluating Radiation Therapy Related Changes in the Prostate. Workshop on Prostate Cancer Imaging (in conjunction with MICCAI). 2011; 6963:80–91.
16. Viswanath, S.; Tiwari, P.; Chappelow, J.; Toth, R.; Kurhanewicz, J.; Madabhushi, A. CADOnc: An integrated toolkit for evaluating radiation therapy related changes in the prostate using multiparametric MRI; Biomedical Imaging: From Nano to Macro 2011 IEEE International Symposium on; 2011. p. 2095-2098.

17. Roberts HR, Paley M, Hall-Craggs MA, Lees WR, Friedman EP, Clemence M, Buonacorssi G, Bown SG. Dynamic magnetic resonance control of interstitial laser photocoagulation therapy of colorectal hepatic metastases. Lancet. 1994; 343(8907):1221. [PubMed: 7909879]
18. Lindner U, Lawrentschuk N, Weersink RA, Davidson SR, Raz O, Hlasny E, Langer DL, Gertner MR, Van der Kwast T, Haider MA, Trachtenberg J. Focal laser ablation for prostate cancer followed by radical prostatectomy: validation of focal therapy and imaging accuracy. Eur Urol. 2010; 57(6):1111–1114. [PubMed: 20346578]
19. Viswanath S, Bloch N, Chappelow J, Toth R, Rofsky N, Genega E, Lenkinski R, Madabhushi A. Central gland and peripheral zone prostate tumors have significantly different quantitative imaging signatures on 3 Tesla endorectal, in vivo T2-weighted MR imagery. J Magn Reson Imaging. 2012; 36(1):213–224. [PubMed: 22337003]
20. Madabhushi A, Udupa JK. New methods of MR image intensity standardization via generalized scale. Medical Physics. 2006; 33(9):3426–3434. [PubMed: 17022239]
21. Madabhushi A, Feldman MD, Metaxas DN, Tomaszeweski J, Chute D. Automated detection of prostatic adenocarcinoma from high-resolution ex vivo MRI. IEEE Trans Med Imaging. 2005; 24(12):1611–1625. [PubMed: 16350920]
22. Chappelow J, Bloch BN, Rofsky N, Genega E, Lenkinski R, DeWolf W, Madabhushi A. Elastic registration of multimodal prostate MRI and histology via multiattribute combined mutual information. Med Phys. 2011; 38(4):2005–2018. [PubMed: 21626933]
23. Viswanath S, Palumbo D, Chappelow J, Patel P, Bloch BN, Rofsky N, Lenkinski R, Genega E, Madabhushi A. Empirical evaluation of bias field correction algorithms for computer-aided detection of prostate cancer on T2w MRI. SPIE Medical Imaging. 2011; 79630 79630V–79630V–12.
24. Nyul L, Udupa J, Zhang X. New variants of a method of mri scale standardization. Medical Imaging, IEEE Transactions on. 2000; 19(2):143–150.
25. Lopes R, Ayache A, Makni N, Puech P, Villers A, Mordon S, Betrouni N. Prostate cancer characterization on MR images using fractal features. Med Phys. 2010; 38(1):83–95. [PubMed: 21361178]
26. Agner SC, Soman S, Libfeld E, McDonald M, Thomas K, Englander S, Rosen MA, Chin D, Nosher J, Madabhushi A. Textural Kinetics: A Novel Dynamic Contrast-Enhanced (DCE)-MRI Feature for Breast Lesion Classification. J Digit Imaging. 2010; 24(3):446–463. [PubMed: 20508965]
27. Wang Y, Chua C-S. Face recognition from 2D and 3D images using 3D Gabor filters. Image and Vision Computing. 2005; 23(11):1018–1028.
28. Haralick RM, Shanmugam K, Dinstein I. Textural Features for Image Classification. IEEE Trans Sys Man Cybernetics. 1973; 3(6):610–621.
29. Pickles MD, Gibbs P, Lowry M, Turnbull LW. Diffusion changes precede size reduction in neoadjuvant treatment of breast cancer. Magnetic Resonance Imaging. 2006; 24(7):843–847. [PubMed: 16916701]

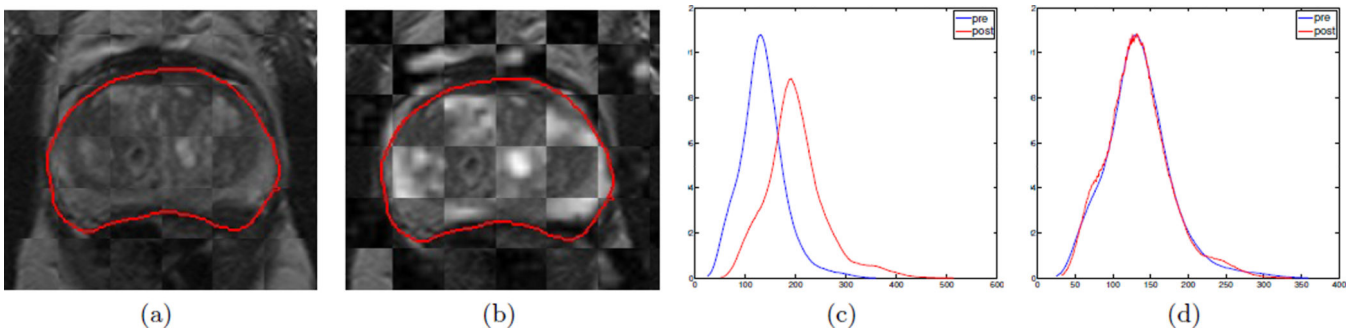

Figure 1.

Checkerboard overlays showing registration results for (a) $\mathscr{C}_{t2}^{post}/\mathscr{C}_{t2}^{pre}$ and (b) $\mathscr{C}_{adc}^{pre}/\mathscr{C}_{t2}^{pre}$. Red outlines on each of (a) and (b) correspond to the prostate capsule segmentation (obtained via expert annotation of the T2w MRI). Note contiguous structures in (a) and (b) denoting successful registrations. (c) Misalignment between intensity distributions for pre- (blue) and post-LITT (red) T2w MRI. (d) After intensity standardization,[20] the intensity distributions are aligned enabling direct comparison of the values.

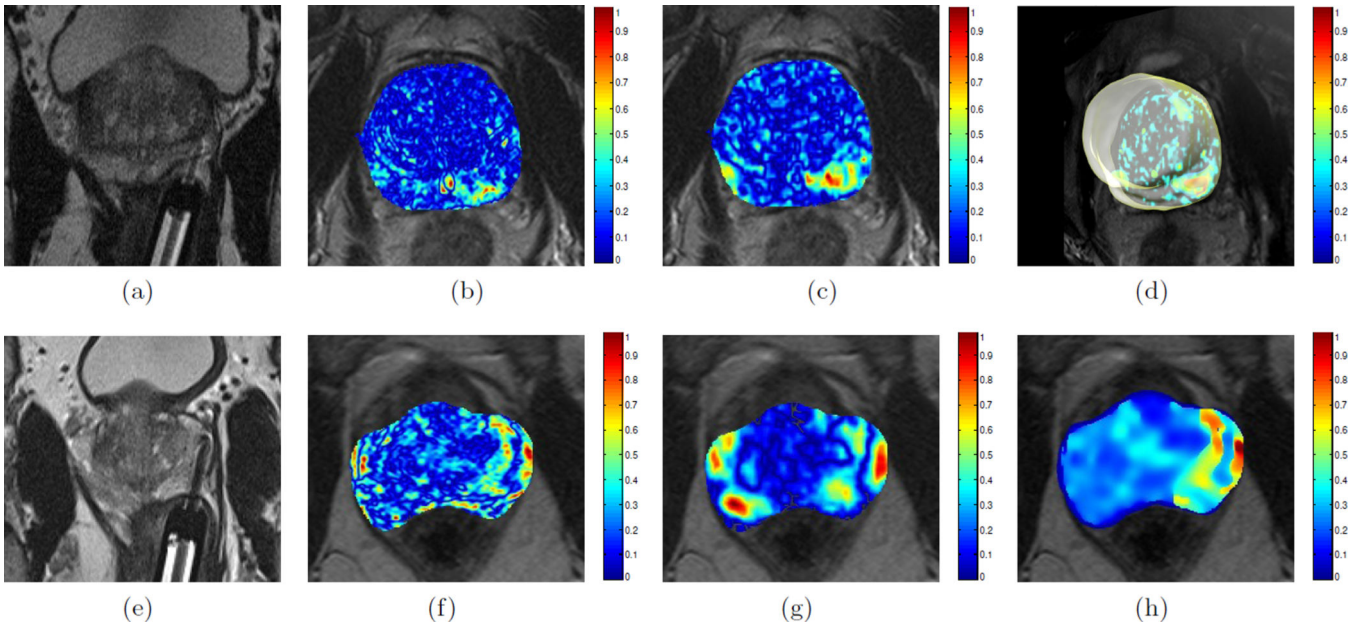

Figure 2.

(a), (e) *In vivo* T2w axial MR image showing region of ablation at the tip of the Visualase laser needle, for 2 different datasets. Representative visualizations of corresponding difference maps: (b), (f) $\mathscr{D}_{t2w}$; (c), (g) $\mathscr{D}_{adc}$; (d), (h) $\mathscr{D}_{int}$. Note that the difference maps show significant change (red) in the regions ablated by the needle (compare against regions ablated in (a) and (e)). Video 1 is a rotating visualization of (d) that demonstrates the LITT-related changes in 3D for this dataset. http://dx.doi.org/doi.number.goes.here

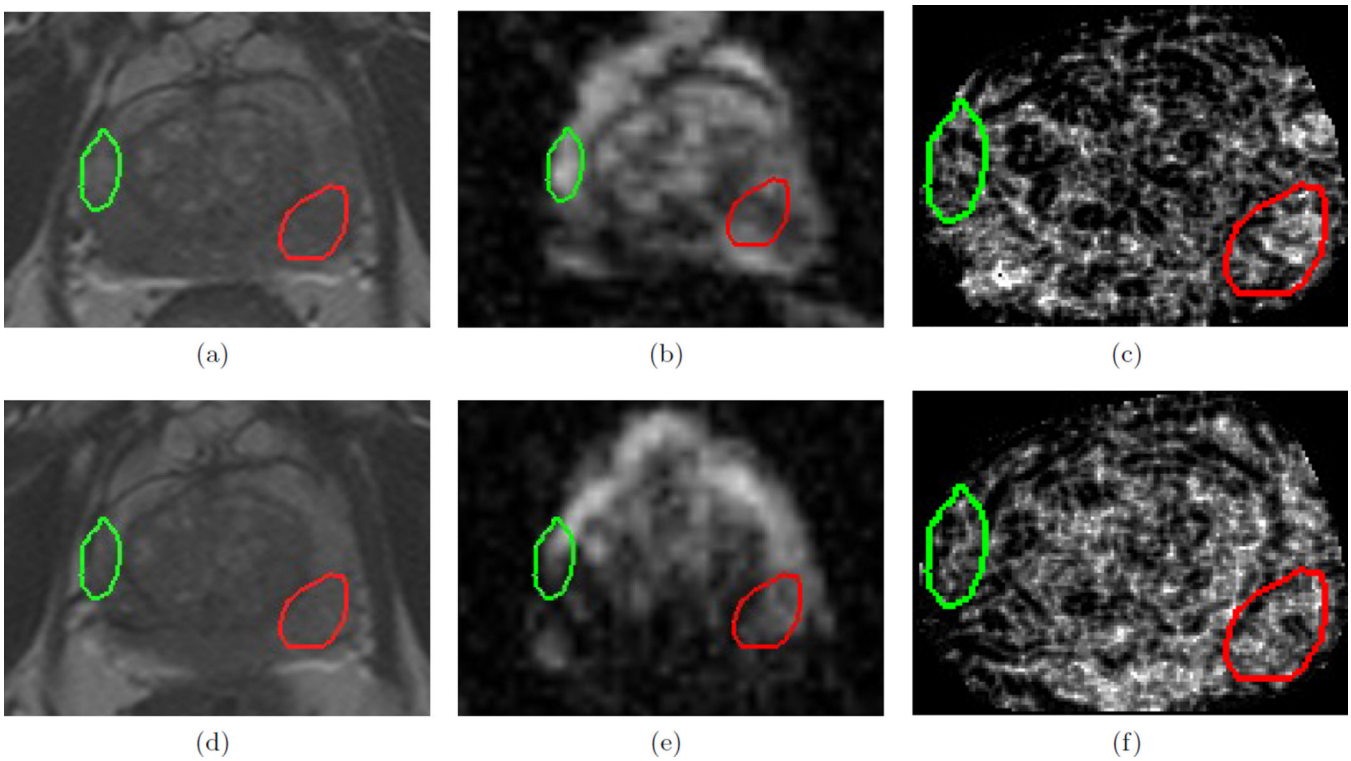

Figure 3.

Images from a single dataset corresponding to representative sections from (a) $\mathscr{C}_{t2w}^{pre}$, (d) $\mathscr{C}_{t2w}^{post}$, (b) $\mathscr{C}_{adc}^{pre}$, (e) $\mathscr{C}_{adc}^{post}$, (c) $\mathscr{C}_{20}^{pre}$, (f) $\mathscr{C}_{20}^{post}$. Green outlines correspond to benign regions ($N(C)$) while red outlines correspond to cancerous regions ($A(C)$), as annotated by a radiologist. While little change is observed within the CaP region (red) between (a) and (d) on T2w MRI, corresponding ADC value appears to change distinctly between (b) and (e). By contrast, the corresponding top-performing T2w feature (Haralick energy) illustrates distinct change within the CaP region (red), low change within benign region (green), as well as a reaction to LITT around the cancerous region illustrated via brighter values around the red outline (compare (c) and (f)).

	ADC value	T2w intensity	T2w Haralick energy
$\Delta^{A,pre}$	-0.452	0.765	**-1.591**
$\Delta^{A,post}$	0.493	1.109	**-0.530**
$\Delta^{N,post}$	1.221	1.751	**-0.499**
$\Delta^{N,post}$	-0.157	1.406	**0.932**

(a)

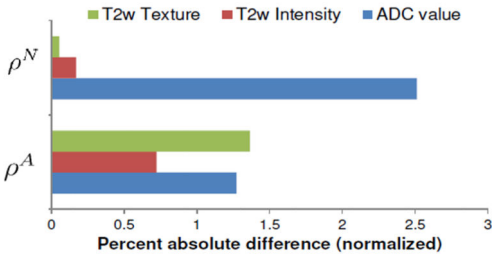

(b)

Figure 4.

(a) Summary of normalized mean values for each of 4 MR parameters, pre- and post-LITT (over all 5 studies). The percent change in each of these parameters (averaged over 5 studies) is visualized as a graph in (b). Based off these results, T2w texture (Haralick energy) appears to provide the best trade-off in detection sensitivity and specificity in quantifying LITT-related MP-MRI changes within the prostate.